

1 The format of this response is as follows:

2

3 In the first part, "Authors' Response to Anonymous Referee 1", we
4 provide a point-by-point response to the referee's comments. We provide each of the
5 referee's comments in **bold font**. After each comment that requires a response we
6 provide a response (in regular font). If we modified the manuscript in response to a
7 comment, we describe what the modification was, and indicate where it was made in the
8 revised manuscript (the revised manuscript is provided at the end of this document).

9

10 In the second part, "Authors' Response to C. van Heerwaarden", we
11 provide a point-by-point response to the referee's comments. We provide each of the
12 referee's comments in **bold font**. After each comment that requires a response we
13 provide a response (in regular font). If we modified the manuscript in response to a
14 comment, we describe what the modification was, and indicate where it was made in the
15 revised manuscript (the revised manuscript is provided at the end of the document).

16

17 In the third part, **Additional modifications to the manuscript**, we describe
18 modifications to the manuscript not made in response to any specific comment of either
19 referee. For the most part these modifications are minor, however we did fix two errors
20 in the final analytical solution (errors in the text, not the code; so these did not affect
21 any of the presented results).

22

23 In the end, we provide the marked up revised manuscript (changed areas are highlighted
24 in yellow).

25

26 Authors' Response to Anonymous Referee 1

27

28 **The authors derive an analytical solution of the two-dimensional steady Boussinesq**
29 **equations in the limit of zero Reynolds number. To obtain this solution they transform the**
30 **equations into a sixth-order equation for the streamfunction. Then they seek a solution in**
31 **the form of a single-harmonic, $A(z)\cos(kx)$. Then the general solution is found as an infinite**
32 **summation of single-harmonic solutions. The procedure is rigorous and well-described. In**
33 **the second part of the paper the authors proceed to use this analytical solutions to test**
34 **different boundary conditions for the pressure Poisson equation in a particular numerical**
35 **implementation. They consider two cases in which they compare numerical results for**
36 **homogeneous and inhomogeneous types boundary conditions for the pressure Poisson**
37 **equation to the analytical solution. Only the inhomogeneous boundary condition passes**
38 **both tests. In summary, this is an interesting paper that deserves publication. I have several**
39 **minor comments:**

40

41 **1. Section 2.1: Please explain the physical meaning of equation (3), i.e. that the equation for**
42 **b is based on the transport equation for the temperature.**

43 Equation (2.3) is the thermal energy equation (differential form of the first law of
44 thermodynamics). In the revised manuscript we now briefly discuss the governing equations,
45 including (2.3) in the paragraph right after (2.4). We also give a reference to where the equations
46 are described more fully (Chandrasekhar 1961). Further down in the paragraph we give a
47 reference (Kundu 1990) for the Brunt-Väisälä frequency N , a parameter that appears in (2.3).

48

49 **2. Please specify which condition has been substituted in which equation in order to obtain**
50 **Eqs. (24-25).**

51 Right before (2.24) we now state that: "In view of (2.7) and (2.17), the impermeability
52 condition $w(x,0) = 0$ and no-slip condition $u(x,0) = 0$ yield"

53

54 **3. Section 2.3: "The derivation of the u field requires considerable effort and is not**
55 **pursued." I do not understand this. As far as I understand, the analytical solution of u is**

56 **simply the analytical partial derivative of Eq. (39) with respect to x , which can be explicitly**
57 **written as an infinite sum. Do I miss anything?**

58 The referee is not quite right. As can be seen from (7), one gets u by differentiating the
59 streamfunction (specified in (39)) with respect to z , not x [One gets w by differentiating the
60 streamfunction with respect to x , and that's a relatively easy calculation]. Moreover, as can be
61 seen from (31), z is implicitly inside four of the factors in (39). This is why obtaining u is
62 potentially complicated.

63 However, we decided to go ahead and take the z -derivative of (39) and see if we could
64 obtain a relatively compact final form for u . It turns out that by making use of addition formulas
65 for sines, the results do simplify considerably and the final form of u is not too bad. So, we now
66 present the analytical solution for u : (2.32) for the single-harmonic wave and (2.41) for the
67 square wave. The differences between the analytical u and the u obtained by finite differencing
68 the streamfunction are visually imperceptible for tests A-1 and A-2. The quantitative changes are
69 generally less than 1 % but are on the order of 1 % near the surface. Our reported values for the
70 R ratios do not change for A-1 but there is a minor change in one of the R ratios for A-2: R_b was
71 originally $R_b \cong 3.6 \times 10^{-3}$ but is now $R_b \cong 3.8 \times 10^{-3}$. The refined value is given in the revised
72 manuscript. With the analytical solution for u now provided, there is now no reason to discuss
73 obtaining the u field by finite-differencing the streamfunction. We have omitted such prose from
74 the revised manuscript.

75

76 **4. Section 3: "The surface condition on pressure is the inhomogeneous Neumann condition**
77 **that arises from projecting the vertical equation of motion into the vertical, and imposing**
78 **the impermeability condition (Vreman, 2014; also see our Appendix)." The sentence can be**
79 **maintained, but a sentence should be added that, in addition, it is important that the**
80 **discretized Poisson equation somehow incorporates the condition that $\delta = \text{div } \mathbf{u} = 0$ on**
81 **the wall or in the direct vicinity of the wall. This was also stressed by Vreman (and others)**
82 **and is briefly mentioned in the appendix. It is good to include this requirement also in the**
83 **main text. In the method of the authors the condition $\delta = 0$ near the wall is probably**
84 **implicitly enforced via the alternative Poisson equation, specified in the Appendix, Eq.**
85 **(A3b). After Eq. (A3b) the authors cite the pressure Poisson equation paradox using a**
86 **sentence of Gresho and Sani. Please mention there that Vreman has revisited this paradox**

87 **and has shown that, at least for the standard staggered method, the discretized version of**
88 **(A3b) (with appropriate Neumann condition) is equivalent to the discretized version of**
89 **(A3a) supplemented with the condition that $\text{div}(\text{Laplacian}(u))=0$ in the direct vicinity of the**
90 **wall. Equipped with the latter the condition, the diffusion equation $d \text{ delta}/dt = \nu * \text{ Laplacian}(\text{delta})$ leads to $\text{delta}=0$ for all time.**

92 Yes, the divergence-free condition near the wall is enforced via the alternative Poisson
93 equation (A3b). We have modified the sentence right after (A3b) to emphasize that this
94 alternative Poisson equation assures that (A2) (the divergence-free condition) is satisfied.

95 Since we want section 3 to focus on the verification tests, we did not want to divert too
96 much attention in that section to the technical details of the pressure equation, pressure boundary
97 condition, and related topics. However, we agree that these details are certainly important and
98 should be clearly discussed. So, as a compromise, we modified a sentence in section 3 to read:
99 "The pressure is diagnosed from a Poisson equation (equation (3b), discussed in the
100 Appendix),..." Then, in the Appendix we modified the sentence about (A3b) enforcing the
101 divergence-free condition (the modification described in the paragraph above) and added two
102 sentences to the discussion of (A3b) along the lines suggested by the referee. Then, after those
103 two new sentences, we end the paragraph with: "We note that (A3b) is the form adopted in our
104 numerical code."

105

106 **5. Section 3: The numerical solutions are obtained on an un-staggered grid. Please explain**
107 **what was done to prevent odd-even decoupling of the pressure. Was the Rhie-Chow**
108 **interpolation method used, for example?**

109 The numerical solutions are obtained on a staggered (Arakawa C) grid so no decoupling
110 of the pressure was occurring/noticed. We now mention "staggered (Arakawa C) grid" in the
111 discussion of the DNS code in section 3.

112

113 **6. Section 3: Please explain the meaning of the abbreviations HNC and INC (I guess**
114 **homogeneous Neumann condition and inhomogeneous Neumann condition).**

115 Yes, HNC is our acronym for homogeneous Neumann condition and INC is our
116 acronym for inhomogeneous Neumann condition. We now introduce these acronyms
117 near the end of the second paragraph of section 3.

118 Authors' Response to Referee C. van Heerwaarden (Referee)

119

120 **General comments**

121 **I recommend minor revisions. The paper presents a validation test for solvers for buoyancy**
122 **driven flows. To the reviewer's knowledge it is the first validation test for wall-bounded**
123 **Boussinesq flows including buoyancy and therefore deserves publishing. I have tested the**
124 **MicroHH (<http://github.com/microhh/microhh>) code against the analytical solution**
125 **provided in the paper and it gives the correct solutions (see attached figures). Nonetheless,**
126 **there are a couple of improvements that could be made. First of all, it would be great if the**
127 **reference cases could be presented in a non-dimensional framework, to make them more**
128 **general. Second, GMD suggests strongly to submit code for benchmarking papers. I would**
129 **appreciate if the authors can provide their code, to enable the readers to use the test case**
130 **with their own code.**

131 We probably should have started the project in non-dimensional form, but since we did
132 not, we are hesitant to recast the theory and code into non-dimensional forms. The changes,
133 while straightforward for both the text and code, would be extensive and thus offer new
134 possibilities for errors to creep in.

135 Yes, we agree that the test code should be freely available. The Fortran code for the
136 analytical solution is now included as a supplement to the article. The code is named "square.f"
137 ("square" because the disturbance is a square wave) and it is configured for Test 1-A. A
138 statement on code availability has been added just before the Acknowledgements statement.

139

140 **Abstract Maybe the authors can stress here that there are very few, or maybe even no**
141 **analytical solutions for wall-bounded buoyancy driven flows around and their paper is**
142 **therefore really a novelty.**

143 In the abstract we have added the sentence: "The analytical solution is one of the
144 few available for wall-bounded buoyancy-driven flows."

145

146 **Page 2850 Can the authors shortly explain how they got to their set of equations?**

147 We have added a few lines describing the individual governing equations. We

148 also give a reference for the equations (Chandrasekhar 1961) and for the Brunt-Väisälä
149 frequency N that appears in the thermal energy equation (Kundu 1990).

150
151 **Page 2857 It would be good if the authors can write some guidelines on how to use their**
152 **validation test with a model with staggered grids. For instance, if \mathbf{u} is interpolated, how fine**
153 **does the analytical solution need to be in order to have reference data for which the error**
154 **in the analytical solution is negligible to the model error?**

155 The analytical solution can easily be output to a staggered grid. If one is coding
156 the analytical solution from scratch (i.e., not using our computer code), one can input x
157 and z locations that coincide with the staggered points. One can use a different set of x
158 and z locations for any of the dependent variables. Our current computer code for the
159 analytical solution is set up to use the same x and z locations for all variables (i.e.,
160 unstaggered arrangement), but it is straightforward to modify that code so the
161 dependent variables are output on any desired grid.

162
163 **Formula 41 Why don't the authors define the first Reynolds number as the vorticity**
164 **advection divided by the vorticity diffusion?**

165 Actually, in a continuum sense, since $\frac{\partial b}{\partial x} = \nu \nabla^2 \eta$ (from equation (2.5)), our

166 definition $R_\eta \equiv \frac{\max |\mathbf{u} \cdot \nabla \eta|}{\max |\partial b / \partial x|}$ is equivalent to the definition suggested by the referee,

167 $R_\eta \equiv \frac{\max |\mathbf{u} \cdot \nabla \eta|}{\max |\nu \nabla^2 \eta|}$. In practice, however, the errors associated with discretizing $\nabla^2 \eta$ may

168 be worse than those associated with discretizing $\partial b / \partial x$, so we prefer our definition.

169
170 **Page 2859 Why are 50.000 terms taken? Isn't this an enormous amount?**

171 Yes, for the two test cases presented the 50000 terms is an enormous amount.
172 However, in the course of the testing (we only showed two tests, but have conducted

173 many additional tests, including tests over larger horizontal domains), we did not want
174 to be burdened by having to go back and rerun a test in case we had too few terms. By
175 choosing such a large number, we removed that parameter from further consideration.

176

177 **Page 2864 Do I understand correctly that the authors underline statements by previous**
178 **papers that models on a staggered grid do not require a pressure boundary condition?**

179 We were trying to be diplomatic in our statements on that page, and believe that the
180 current phrasing in the original manuscript is accurate, but we do not want to make too much out
181 of it. In going through both engineering and meteorological modeling literature, we were struck
182 at how often key details related to the pressure boundary condition were glossed over or omitted.
183 In many cases it was not possible to determine what was actually implemented.

184

185 **Page 2865 In the last statement the authors mention the numerical boundary layers. Are**
186 **these a problem in explicit codes as they are using as well, or does this problem only play a**
187 **role in case implicit diffusion has to be applied?**

188 We did not observe the development of thin numerical boundary layers in any of our
189 tests. However, we don't know whether this is because our code is explicit or is related to the
190 nature of the test flows we considered. The thin numerical boundary layers reported in the
191 literature have generally been for test flows dominated by advection rather than diffusion.

192

193 **Figure 6 Why are the results asymmetric? You are solving a purely symmetric system.**
194 **Which process introduces the asymmetry in the solution?**

195 The asymmetry is a result of nonlinearities in the numerically simulated flow. By
196 the time the numerical solution has evolved to the point shown in Figure 6, the flow is
197 no longer in a linear regime. If we consider the motion in one convective cell we have an
198 ascending warm branch and a descending cooler branch, which would be symmetric if
199 the system remained linear (and of course it is linear/symmetric in the analytical test
200 case). However, in the numerically simulated flow, the (positive) buoyancy in the rising
201 branch is transported laterally (nonlinear advection) at the top of the circulation cell to
202 the top of the descending cell. This introduces an asymmetry to the circulation. Once

203 the symmetry of the flow is broken, the flow can become quite complicated.

204

205

206 Additional modifications to the manuscript (i.e., not made in
207 response to the reviewers' comments)

208

209 Please note that the third author would like his middle initial "A" included in his name:
210 Jeremy A. Gibbs.

211

212 We have added a new reference: Egger (1981). The Egger study was related to ours in
213 that it was concerned with a linear analysis of the 2D Boussinesq governing equations
214 for thermally driven flow. Egger's analysis was largely for slope flows, though with flat
215 terrain (our focus) considered as a special case. However, Egger outlines how to get the
216 analytical solution but does not actually provide the final analytical solution. We
217 mention this Egger study in the second paragraph of Section 1. We also mention it in
218 the paragraph right after (2.8): the restriction on acceptable surface buoyancies
219 described in that paragraph was first noted by Egger, though without details.

220

221 A correction was made to the original equations (2.39) and (2.40) [these now appear as
222 equations (2.40) and (2.42), respectively]. The factor $k^{1/3}$ in the denominator of the
223 term in front of the summation in (2.39) and the factor $k^{2/3}$ in the numerator of the
224 term in front of the summation in (2.40) should be kept inside the summations. These
225 factors were treated correctly in the computer code, so none of the presented results
226 were affected.

227

228 Section 3. We now make the number of points in the x and z direction unambiguous:

229 instead of writing the number of points in test A-1 as (513, 1025) we write, "...consisted
230 of 513 points in the x direction and 1025 points in the z direction,..." Similarly, for test
231 A-2, we now write, "...was generated with 2049 points in the x direction and 513 points
232 in the z direction,..."

233

234 In the Appendix we now write the time step as Δt instead of δt since the symbol δ
235 has already been used to represent the divergence of the velocity field.

236

237 In several places in the manuscript we now use bold to indicate the vector \mathbf{u} (formerly
238 we used \vec{u}).

239

240 We have slightly modified the acknowledgements statement (we now thank the
241 anonymous reviewer).

242

243 **An analytical verification test for numerically simulated convective flow**

244 **above a thermally heterogeneous surface**

245 by Alan Shapiro, Evgeni Fedorovich, and Jeremy **A.** Gibbs

246

247 **Abstract.** An analytical solution of the Boussinesq equations for the motion of a
248 viscous stably stratified fluid driven by a surface thermal forcing with large horizontal
249 gradients (step changes) is obtained. **This analytical solution is one of the few available**
250 **for wall-bounded buoyancy-driven flows.** The solution can be used to verify that
251 computer codes for Boussinesq fluid system simulations are free of errors in formulation
252 of wall boundary **conditions** and to evaluate the relative performances of competing
253 numerical algorithms. Because the solution pertains to flows driven by a surface thermal
254 forcing, one of its main applications may be for testing the no-slip, impermeable wall
255 boundary conditions for the pressure Poisson equation. Examples of such tests are
256 presented.

257 1 Introduction

258 Thermal disturbances associated with variations in underlying surface properties can
259 drive local circulations in the atmospheric boundary layer (Atkinson, 1981; Briggs, 1988;
260 Hadfield et al., 1991; Segal and Arritt, 1992; Simpson, 1994; Mahrt et al., 1994; Pielke,
261 2001; McPherson, 2007; Kang et al., 2012) and affect the development of the convective
262 boundary layer (Patton et al., 2005; van Heerwaarden et al., 2014). Computational fluid
263 dynamics (CFD) codes for modeling such flows commonly solve the Boussinesq
264 equations of motion and thermal energy for a viscous/diffusive stably stratified fluid. In
265 this paper we present an analytical solution of the Boussinesq equations for flows driven
266 by a surface thermal forcing with large gradients (step changes) in the horizontal. The
267 solution can be used to verify that CFD codes for Boussinesq fluid system simulations
268 are free of errors, and to evaluate the relative performances of competing numerical
269 algorithms. Such verification procedures are important in the development of CFD
270 models designed for research, operational, and classroom applications.

271 We solve the linearized Navier-Stokes and thermal energy equations analytically
272 for the case where the surface buoyancy varies laterally as a square wave (Fig. 1).
273 Attention is restricted to the steady state. No boundary-layer approximations are made;
274 the solution is non-hydrostatic, and both horizontal and vertical derivatives are included
275 in the viscous stress and thermal diffusion terms. The solution is similar to that of
276 Axelsen et al. (2010) for katabatic flow above a cold strip, but is easier to evaluate (no

277 slope present) and applies to the more general scenario where the viscosity and
278 diffusivity coefficients can differ. The flow is also similar to a special case (no slope)
279 considered by Egger (1981), although a final analytical solution was not provided in
280 that study. Strictly speaking, the linearized Navier-Stokes equations apply to a class of
281 very low Reynolds number motions known as creeping flows. Such flows appear in
282 studies of lubrication, locomotion of microorganisms, lava flow, and flow in porous
283 media. Of course, for the task at hand, if our linear solution is to serve as a benchmark
284 for a nonlinear numerical model solution, it is essential that the parameter space be
285 restricted to values for which the model's nonlinear terms are negligible.

286 Because the solution pertains to flows driven by a surface thermal forcing, one of
287 its main applications may be as a test for surface boundary conditions in the pressure
288 Poisson equation. In models of atmospheric boundary-layer flows, the buoyancy is a
289 major contributor to the forcing term in the Poisson equation and also appears in the
290 associated surface boundary condition. The pressure boundary condition on a solid
291 boundary in incompressible (Boussinesq) fluid flows is an important and complex issue
292 that has long been fraught with technical difficulties and controversies (Strikwerda,
293 1984; Orszag et al., 1986; Gresho and Sani, 1987; Gresho, 1990; Temam, 1991; Henshaw,
294 1994; Petersson, 2001; Sani et al., 2006; Rempfer, 2006; Guermond et al., 2006;
295 Nordström et al., 2007; Shirokoff and Rosales, 2011; Hosseini and Feng, 2011; Vreman,
296 2014). Typical fractional-step solution methodologies and associated pressure (or

297 pseudo-pressure) boundary-condition implementations are often verified using various
298 prototypic flows such as Poiseuille flows, lid-driven cavity flows, flows over cylinders or
299 bluff bodies, viscously decaying vortices, and dam-break flows. We are unaware of
300 verification tests in which flows were driven by a heterogeneous surface buoyancy
301 forcing. Our solution is designed to fill this gap.

302 The analytical solution is derived in Sect. 2. In Sect. 3, this solution is compared
303 to numerically simulated fields in a steady state. Two versions of a numerical code are
304 run: a version in which the correct surface pressure boundary condition is applied, and a
305 version in which the pressure condition is mis-specified. A summary follows in Sect. 4.

306

307 **2 Analytical solution**

308 We derive the solution for steady flow over an underlying surface along which the
309 buoyancy varies laterally as a single harmonic function. This single-harmonic solution is
310 then used as a building block in a Fourier representation of the square-wave solution.

311

312 **2.1 Governing equations**

313 Consider the flow of a viscous stably stratified fluid that fills the semi-infinite domain
314 above a solid horizontal surface (placed at $z = 0$). This surface undergoes a steady
315 thermal forcing that varies periodically in the right-hand Cartesian x direction, but is
316 independent of the y direction. The two-dimensional (x, z) flow is periodic in x , and

317 satisfies the linearized (assuming the disturbance is of small amplitude) governing
 318 equations under the Boussinesq approximation,

$$319 \quad 0 = -\frac{\partial \Pi}{\partial x} + \nu \nabla^2 u, \quad (2.1)$$

$$320 \quad 0 = -\frac{\partial \Pi}{\partial z} + b + \nu \nabla^2 w, \quad (2.2)$$

$$321 \quad 0 = -N^2 w + \alpha \nabla^2 b, \quad (2.3)$$

$$322 \quad \frac{\partial u}{\partial x} + \frac{\partial w}{\partial z} = 0. \quad (2.4)$$

323 Apart from notational differences, (2.1)–(2.4) are the two-dimensional steady state
 324 versions of (55)–(57) of Sect. II of Chandrasekhar (1961). Equations (2.1) and (2.2) are
 325 the horizontal (x) and vertical (z) equations of motion, respectively, (2.3) is the thermal
 326 energy equation (differential form of the first law of thermodynamics) expressed in
 327 terms of the buoyancy variable (defined below), and (2.4) is the incompressibility
 328 condition. Here u and w are the horizontal and vertical velocity components, $\Pi \equiv$
 329 $[p - p_e(z)]/\rho_w$ is the kinematic pressure perturbation [p is pressure, $p_e(z)$ is pressure in a
 330 hydrostatic environmental state in which the density profile is $\rho_e(z)$, ρ_w is a constant
 331 reference density, say, $\rho_e(0)$], and $b \equiv -g[\rho - \rho_e(z)]/\rho_w$ is the buoyancy, where ρ is the
 332 actual density, and g is the acceleration due to gravity. The Brunt-Väisälä frequency
 333 $N \equiv \sqrt{-(g/\rho_w)d\rho_e/dz}$ of the ambient fluid (Kundu 1990), kinematic viscosity ν , and
 334 thermal diffusivity α are taken constant.

335 We obtain our solution using a standard vorticity/streamfunction formulation.

336 Cross-differentiating (2.1) and (2.2) yields the vorticity equation,

$$337 \quad 0 = -\frac{\partial b}{\partial x} + \nu \nabla^2 \eta, \quad (2.5)$$

338 where $\eta \equiv \partial u / \partial z - \partial w / \partial x$ is the vorticity. Eliminating b from (2.3) and (2.5) yields

$$339 \quad \nabla^4 \eta = \frac{N^2}{\nu \alpha} \frac{\partial w}{\partial x}. \quad (2.6)$$

340 Introducing a streamfunction ψ defined through

$$341 \quad u = \partial \psi / \partial z, \quad w = -\partial \psi / \partial x, \quad (2.7)$$

342 guarantees that (2.4) is satisfied, and transforms (2.6) into a single equation for ψ ,

$$343 \quad \nabla^6 \psi + \frac{N^2}{\nu \alpha} \frac{\partial^2 \psi}{\partial x^2} = 0. \quad (2.8)$$

344 The dependent variables are assumed to vanish far above the surface ($z \rightarrow \infty$). On the

345 surface we apply no-slip ($u = 0$) and impermeability ($w = 0$) conditions, and specify a

346 periodic (in x) buoyancy distribution. As we will now see, restricting the dependent

347 variables to steady periodic forms that vanish as $z \rightarrow \infty$ also restricts acceptable

348 distributions of the surface buoyancy. The restriction was first noted by Egger (1981,

349 Sect. 3c), though without details. Averaging (2.3) over one period (using $w = -\partial \psi / \partial x$)

350 yields $d^2 \bar{b} / dz^2 = 0$, which integrates to $\bar{b} = A + Bz$ (\bar{b} is the average of b ; A and B are

351 constants). Taking $b \rightarrow 0$ as $z \rightarrow \infty$, implies that $\bar{b} \rightarrow 0$ as $z \rightarrow \infty$, in which case $A =$

352 $B = 0$, and $\bar{b}(z) = 0$. In particular, at the surface, $\bar{b}(0) = 0$. If a surface distribution

353 $b(x,0)$ violates this condition, the ground acts as a net heat source/sink. In an unsteady
 354 model, such a source/sink would force a continually upward-developing disturbance, and
 355 a steady state could never be attained.

356

357 2.2 Single-harmonic forcing

358 For a surface buoyancy of the form $b(x,0) \propto \sin kx$, (2.3) indicates that ψ is of the form

$$359 \quad \psi = A(z) \cos kx. \quad (2.9)$$

360 Application of (2.9) in (2.8) yields

$$361 \quad \left(\frac{d^2}{dz^2} - k^2 \right)^3 A - \frac{N^2 k^2}{\nu \alpha} A = 0, \quad (2.10)$$

362 which has solutions of the form $A \propto e^{Mz}$ for M satisfying

$$363 \quad (M^2 - k^2)^3 = \frac{N^2 k^2}{\nu \alpha}. \quad (2.11)$$

364 Taking the one-third power of (2.11) yields a useful intermediate result:

$$365 \quad M^2 - k^2 = \frac{N^{2/3} k^{2/3}}{\nu^{1/3} \alpha^{1/3}} e^{2n\pi i/3}, \quad (2.12)$$

366 where n is an integer. Rearranging (2.12) and taking the square root yields

$$367 \quad M = \pm \sqrt{k^2 + \frac{N^{2/3} k^{2/3}}{\nu^{1/3} \alpha^{1/3}} e^{2n\pi i/3}}. \quad (2.13)$$

368 Equation (2.13) furnishes six roots, two for each of $n = 0, 1, 2$. To ensure that $A(z) \rightarrow 0$

369 as $z \rightarrow \infty$, we reject the roots with a positive real part. With the radicand of (2.13)

370 expressed in polar form, the physically acceptable roots are

$$371 \quad M_0 = -\sqrt{k^2 + \frac{N^{2/3}k^{2/3}}{\nu^{1/3}\alpha^{1/3}}}, \quad (n = 0), \quad (2.14a)$$

$$372 \quad M_1 = -r^{1/2}e^{i\phi/2}, \quad (n = 1), \quad (2.14b)$$

$$373 \quad M_2 = -r^{1/2}e^{-i\phi/2}, \quad (n = 2), \quad (2.14c)$$

374 where the subscript on M denotes the associated value of n , and r and ϕ are defined by

$$375 \quad r \equiv \sqrt{\left[k^2 + \frac{N^{2/3}k^{2/3}}{\nu^{1/3}\alpha^{1/3}} \cos\left(\frac{2\pi}{3}\right)\right]^2 + \left[\frac{N^{2/3}k^{2/3}}{\nu^{1/3}\alpha^{1/3}} \sin\left(\frac{2\pi}{3}\right)\right]^2}, \quad (2.15)$$

$$376 \quad \cos \phi = \frac{1}{r} \left[k^2 + \frac{N^{2/3}k^{2/3}}{\nu^{1/3}\alpha^{1/3}} \cos\left(\frac{2\pi}{3}\right) \right], \quad \sin \phi = \frac{1}{r} \left(\frac{N^{2/3}k^{2/3}}{\nu^{1/3}\alpha^{1/3}} \right) \sin\left(\frac{2\pi}{3}\right) > 0. \quad (2.16)$$

377 **While** solving (2.16) for ϕ , care must be taken when evaluating arcsin or arccos
 378 functions that ϕ appears in the correct quadrant (ϕ should be in quadrant I or II so
 379 $\phi/2$ should always be in quadrant I). Also note from (2.14b) and (2.14c) that M_2 is the
 380 complex conjugate of M_1 ($M_2 = M_1^*$), a fact that will often be used below.

381 With the general solution for ψ written as

$$382 \quad \psi = (B e^{M_0 z} + C e^{M_1 z} + D e^{M_2 z}) \cos kx, \quad (2.17)$$

383 where B , C , and D are constants, the vorticity becomes,

$$384 \quad \eta = \left[B(M_0^2 - k^2) e^{M_0 z} + C(M_1^2 - k^2) e^{M_1 z} + D(M_2^2 - k^2) e^{M_2 z} \right] \cos kx, \quad (2.18)$$

385 and the buoyancy follows from (2.3) as

386
$$b = \frac{kN^2}{\alpha} \left(\frac{B}{M_0^2 - k^2} e^{M_0 z} + \frac{C}{M_1^2 - k^2} e^{M_1 z} + \frac{D}{M_2^2 - k^2} e^{M_2 z} \right) \sin kx + b_h, \quad (2.19)$$

387 where $\nabla^2 b_h = 0$. In view of (2.12), equation (2.19) becomes

388
$$b = \frac{k^{1/3} \nu^{1/3} N^{4/3}}{\alpha^{2/3}} (B e^{M_0 z} + e^{-2\pi i/3} C e^{M_1 z} + e^{-4\pi i/3} D e^{M_2 z}) \sin kx + b_h. \quad (2.20)$$

389 Applying (2.18) and (2.20) in (2.5) yields an equation for $\partial b_h / \partial x$, which upon use of

390 (2.12) and $M_2 = M_1^*$ reduces to $\partial b_h / \partial x = 0$. So b_h is, at most, a function of z . Since

391 $\nabla^2 b_h = 0$, b_h is, at most, a linear function of z , and since b should vanish as $z \rightarrow \infty$,

392 that linear function must be 0. Thus, $b_h = 0$.

393 The pressure follows from (2.1) and (2.12) as

394
$$\Pi = \frac{\nu^{2/3} N^{2/3}}{k^{1/3} \alpha^{1/3}} (B M_0 e^{M_0 z} + C M_1 e^{2\pi i/3} e^{M_1 z} + D M_2 e^{4\pi i/3} e^{M_2 z}) \sin kx + G(z), \quad (2.21)$$

395 where $G(z)$ is a function of integration. Applying (2.21) in (2.2), and using (2.11) yields

396 $dG/dz = 0$, so G is constant. For Π to vanish as $z \rightarrow \infty$, this constant must be zero.

397 The surface conditions determine B , C , and D . The surface buoyancy is

398
$$b(x, 0) = b_0 \sin kx, \quad (2.22)$$

399 where b_0 is a constant forcing amplitude. Application of (2.20) in (2.22) yields

400
$$B + e^{-2\pi i/3} C + e^{-4\pi i/3} D = \frac{b_0 \alpha^{2/3}}{k^{1/3} \nu^{1/3} N^{4/3}}. \quad (2.23)$$

401 In view of (2.7) and (2.17), the impermeability condition $w(x, 0) = 0$ and no-slip

402 condition $u(x,0) = 0$ yield

403
$$B + C + D = 0, \tag{2.24}$$

404
$$BM_0 + CM_1 + DM_2 = 0. \tag{2.25}$$

405 Straightforward but lengthy manipulations yield the solution of (2.23)–(2.25):

406
$$B = - \left(\frac{b_0 \alpha^{2/3}}{\sqrt{3} k^{1/3} \nu^{1/3} N^{4/3}} \right) \frac{2r^{1/2} \sin(\phi/2)}{M_0 + 2r^{1/2} \cos(\pi/3 + \phi/2)}, \tag{2.26}$$

407
$$C = -i \left(\frac{b_0 \alpha^{2/3}}{\sqrt{3} k^{1/3} \nu^{1/3} N^{4/3}} \right) \frac{M_2 - M_0}{M_0 + 2r^{1/2} \cos(\pi/3 + \phi/2)}, \tag{2.27}$$

408
$$D = i \left(\frac{b_0 \alpha^{2/3}}{\sqrt{3} k^{1/3} \nu^{1/3} N^{4/3}} \right) \frac{M_1 - M_0}{M_0 + 2r^{1/2} \cos(\pi/3 + \phi/2)}. \tag{2.28}$$

409 Applying (2.26)–(2.28) in (2.17), (2.20), and (2.18), with (2.12) used in the latter
 410 equation, and noting that B is real, while $D = C^*$ (since $M_2 = M_1^*$), we obtain

411
$$b = \frac{2b_0}{\sqrt{3}} \frac{e^{-Z_c} [\mu \cos(Z_s + \pi/6) + \cos(Z_s + \pi/6 + \phi/2)] - e^{M_0 z} \sin(\phi/2)}{\mu + 2 \cos(\pi/3 + \phi/2)} \sin kx, \tag{2.29}$$

412
$$\psi = \frac{2b_0 \alpha^{2/3}}{\sqrt{3} k^{1/3} \nu^{1/3} N^{4/3}} \frac{e^{-Z_c} [\mu \sin Z_s + \sin(Z_s + \phi/2)] - e^{M_0 z} \sin(\phi/2)}{\mu + 2 \cos(\pi/3 + \phi/2)} \cos kx, \tag{2.30}$$

413 where

414
$$Z_s \equiv z r^{1/2} \sin(\phi/2), \quad Z_c \equiv z r^{1/2} \cos(\phi/2), \quad \mu \equiv M_0 / r^{1/2}. \tag{2.31}$$

415 Application of (2.30) in (2.7) yields the velocity components as

$$416 \quad u = \frac{2b_0 \alpha^{2/3} r^{1/2}}{\sqrt{3} k^{1/3} \nu^{1/3} N^{4/3}} \frac{e^{-Z_c} [\mu \sin(\phi/2 - Z_s) - \sin Z_s] - \mu e^{M_0 z} \sin(\phi/2)}{\mu + 2 \cos(\pi/3 + \phi/2)} \cos kx \quad (2.32)$$

$$417 \quad w = \frac{2b_0 \alpha^{2/3} k^{2/3}}{\sqrt{3} \nu^{1/3} N^{4/3}} \frac{e^{-Z_c} [\mu \sin Z_s + \sin(Z_s + \phi/2)] - e^{M_0 z} \sin(\phi/2)}{\mu + 2 \cos(\pi/3 + \phi/2)} \sin kx. \quad (2.33)$$

418

419 2.3 Piecewise constant (square wave) forcing

420 Next, consider the case where the surface buoyancy varies horizontally as a square

421 wave, with a distribution over one period L given by

$$422 \quad b(x, 0) = \begin{cases} b_{\max}, & 0 < x < L/2, \\ -b_{\max}, & L/2 < x < L. \end{cases} \quad (2.34)$$

423 Such a distribution can be expressed as the Fourier series:

$$424 \quad b(x, 0) = \sum_{n=1}^{\infty} b_n \sin\left(\frac{n\pi x}{L}\right), \quad (2.35)$$

$$425 \quad b_n = \frac{2}{L} \int_0^L b(x, 0) \sin\left(\frac{n\pi x}{L}\right) dx. \quad (2.36)$$

426 Application of (2.34) in (2.36) yields

$$427 \quad b_n = \frac{2b_{\max}}{n\pi} [1 - 2 \cos(n\pi/2) + \cos(n\pi)]. \quad (2.37)$$

428 The solutions for b , ψ , u , and w can then be written as summations over the single-

429 harmonic solutions (2.29), (2.30), (2.32), and (2.33), with k related to n by

$$430 \quad k = \frac{n\pi}{L}, \quad (2.38)$$

431 and with b_0 replaced by b_n :

$$432 \quad b = \frac{2}{\sqrt{3}} \sum_{n=1}^{\infty} b_n \frac{e^{-Z_c} [\mu \cos(Z_s + \pi/6) + \cos(Z_s + \pi/6 + \phi/2)] - e^{M_0 z} \sin(\phi/2)}{\mu + 2 \cos(\pi/3 + \phi/2)} \sin\left(\frac{n\pi x}{L}\right), \quad (2.39)$$

$$433 \quad \psi = \frac{2\alpha^{2/3}}{\sqrt{3}\nu^{1/3}N^{4/3}} \sum_{n=1}^{\infty} \frac{b_n}{k^{1/3}} \frac{e^{-Z_c} [\mu \sin Z_s + \sin(Z_s + \phi/2)] - e^{M_0 z} \sin(\phi/2)}{\mu + 2 \cos(\pi/3 + \phi/2)} \cos\left(\frac{n\pi x}{L}\right), \quad (2.40)$$

$$434 \quad u = \frac{2\alpha^{2/3}}{\sqrt{3}\nu^{1/3}N^{4/3}} \sum_{n=1}^{\infty} b_n \frac{r^{1/2}}{k^{1/3}} \frac{e^{-Z_c} [\mu \sin(\phi/2 - Z_s) - \sin Z_s] - \mu e^{M_0 z} \sin(\phi/2)}{\mu + 2 \cos(\pi/3 + \phi/2)} \cos\left(\frac{n\pi x}{L}\right), \quad (2.41)$$

$$435 \quad w = \frac{2\alpha^{2/3}}{\sqrt{3}\nu^{1/3}N^{4/3}} \sum_{n=1}^{\infty} b_n k^{2/3} \frac{e^{-Z_c} [\mu \sin Z_s + \sin(Z_s + \phi/2)] - e^{M_0 z} \sin(\phi/2)}{\mu + 2 \cos(\pi/3 + \phi/2)} \sin\left(\frac{n\pi x}{L}\right). \quad (2.42)$$

436

437 **3 Verification tests**

438 A solution of the linearized equations may be used to verify a nonlinear code if the

439 nonlinear terms are sufficiently small. Unfortunately, *a priori* estimates of such terms

440 expressed, for example, through a Reynolds number, are not straightforward since the

441 relevant velocity and length scales in our problem are only evident after a solution has

442 been obtained. We thus seek an appropriate set of test parameters through trial and

443 error, guided by *a posteriori* linear solution estimates of the terms $\mathbf{u} \cdot \nabla b$ and $\mathbf{u} \cdot \nabla \eta$

444 $[\mathbf{u} = (u, w)]$ present in nonlinear versions of (2.3) and (2.5), respectively. Specifically, for

445 any computed candidate solution, we formed the ratios of the largest values of those

446 nonlinear terms to the largest values of the corresponding linear terms, that is, the

447 terms actually present in (2.3) and (2.5). We need only consider one such linear term
 448 per ratio since (2.3) and (2.5) are comprised of two terms of equal magnitude. A
 449 solution was deemed to be sufficiently linear if

$$450 \quad R_\eta \equiv \frac{\max|\mathbf{u} \cdot \nabla \eta|}{\max|\partial b / \partial x|} < \varepsilon, \quad \text{and} \quad R_b \equiv \frac{\max|\mathbf{u} \cdot \nabla b|}{\max|\alpha \nabla^2 b|} < \varepsilon, \quad (3.1)$$

451 where ε ($\ll 1$) is a prescribed threshold. The suitability of this approach was
 452 confirmed by the very close agreement between the analytical solutions and the
 453 numerical solutions obtained with the correct surface pressure condition.

454 The numerical model employed in our tests is a variant of a direct numerical
 455 simulation (DNS) code used in the boundary-layer and slope-flow studies of Fedorovich
 456 et al. (2001), Fedorovich and Shapiro (2009a,b), and Shapiro and Fedorovich (2013,
 457 2014). The model solves the Boussinesq governing equations on a staggered (Arakawa
 458 C) grid. Although designed for three-dimensional simulations, the model was run in a
 459 two-dimensional (x, z) mode. The overall solution procedure is patterned on a fractional
 460 step method proposed by Chorin (1968). In our version, the prognostic equations are
 461 integrated using a filtered leapfrog scheme with explicit treatment of the viscous term.
 462 The pressure is diagnosed from a Poisson equation (equation (A3b), discussed in the
 463 Appendix), which is solved using a fast Fourier transform technique in horizontal
 464 planes, and a tridiagonal matrix inversion in the vertical. The surface condition on
 465 pressure is the inhomogeneous Neumann condition (INC) that arises from projecting the

466 vertical equation of motion into the vertical, and imposing the impermeability condition
467 (Vreman, 2014; also see the Appendix). We also run a version of the code in which the
468 surface pressure condition is mis-specified as a homogeneous Neumann condition (HNC).
469 We hasten to add, however, that our implementation of the HNC may be quite different
470 from implementations described in the literature. We elaborate on these technical
471 differences and review general aspects of the problem of surface pressure specification in
472 the Appendix.

473 The analytical solution was evaluated on an un-staggered (x, z) grid extending
474 over one period of the square wave ($x = 0$ to $x = L$). The series were truncated at
475 50000 terms. The governing parameters were adjusted so that the linearity criteria
476 were satisfied in comparisons with $\varepsilon = 5 \times 10^{-3}$.

477 In the first test, we set $\nu = \alpha = 0.001 \text{ m}^2 \text{ s}^{-1}$, $N = 0.02 \text{ s}^{-1}$, $L = 5.12 \text{ m}$, and b_{\max}
478 $= 1 \times 10^{-5} \text{ m s}^{-2}$. For the analytical solution A-1, the (x, z) grid consisted of 513 points
479 in the x direction and 1025 points in the z direction, with grid spacings
480 $\Delta x = \Delta z = 0.01 \text{ m}$. The linearity criteria (3.1) were satisfied with $R_\eta \cong 8.2 \times 10^{-5}$ and
481 $R_b \cong 2.8 \times 10^{-3}$. The analytical b and w fields shown in Fig. 2 depict a broad zone of
482 ascent above the warm surface and a compensating zone of descent over the cold
483 surface, roughly for $z < 1.8 \text{ m}$. In the upper part of these zones (at roughly
484 $0.9 \text{ m} < z < 1.8 \text{ m}$), adiabatic expansion/compression has reversed the senses of the

485 buoyancy fields. Surprisingly, the numerical fields in the inhomogeneous INC-1 and
 486 homogeneous HNC-1 cases are very similar to each other and to the A-1 fields. The u
 487 fields from A-1, INC-1, and HNC-1 shown in Fig. 3 are visually indistinguishable from
 488 one another.

489 To understand why the INC-1 and HNC-1 simulations are so similar, and to
 490 identify simulation parameters that might evince more substantial differences, we
 491 consider the idealized problem in which a specified buoyancy $b = b_0 e^{-\gamma z} \sin kx$ ($\gamma = h^{-1}$,
 492 where h is the e-folding depth scale) is the only forcing term in the Poisson equation
 493 $\nabla^2 \Pi = \partial b / \partial z$, with Neumann surface condition $\partial \Pi / \partial z|_0 = b(x, 0)$. This idealized
 494 problem is solved as

$$495 \quad \Pi_{\text{INC}}^* = \frac{b_0}{\gamma^2 - k^2} \left(k e^{-kz} - \gamma e^{-\gamma z} \right) \sin kx. \quad (3.2)$$

496 The corresponding solution obtained with the homogeneous Neumann condition,
 497 $\partial \Pi / \partial z|_0 = 0$, is

$$498 \quad \Pi_{\text{HNC}}^* = \frac{b_0}{\gamma^2 - k^2} \left(\frac{\gamma^2}{k} e^{-kz} - \gamma e^{-\gamma z} \right) \sin kx. \quad (3.3)$$

499 The relative error (RE) in the vertical pressure gradient force associated with (3.2) and
 500 (3.3), defined as the local absolute error in that force divided by the local buoyancy, is
 501 calculated as

502
$$RE \equiv \left| \frac{\partial \Pi_{\text{INC}}^* / \partial z - \partial \Pi_{\text{HNC}}^* / \partial z}{b} \right| = e^{(a-1)kz}, \quad (3.4)$$

503 where $a \equiv \gamma/k$. Written in terms of the depth scale h and wavelength $\lambda = 2\pi/k$, a can
 504 be interpreted as an aspect ratio characterizing the width to depth scales of the
 505 disturbance, $a = \lambda/(2\pi h) \propto \lambda\gamma$. From (3.4) we see that RE decreases exponentially with
 506 z for disturbances characterized by small aspect ratios, $a < 1$ (which we refer to as deep
 507 disturbances) and increases exponentially with z for disturbances characterized by large
 508 aspect ratios, $a > 1$ (which we refer to as shallow disturbances). The buoyancy in Fig. 2
 509 is suggestive of $a < 1$, which indicates that the first test could be classified as a deep
 510 (error-forgiving) simulation.

511 The preceding analysis suggests that simulations with shallow thermal
 512 disturbances ($a > 1$) might yield large differences between cases with inhomogeneous
 513 and homogeneous Neumann conditions. There did not appear to be a straightforward
 514 way to increase the effective a by systematically varying the parameters (e.g., increasing
 515 L tended to increase the effective h), but a set of suitable parameters were identified
 516 through trial and error and were used as the basis for the second test case.

517 In the second test, we set $\nu = \alpha = 0.0001 \text{ m}^2 \text{ s}^{-1}$, $N = 0.2 \text{ s}^{-1}$, $L = 10.24 \text{ m}$, and
 518 $b_{\text{max}} = 5 \times 10^{-6} \text{ ms}^{-2}$. The analytical solution A-2 was generated with 2049 points in the
 519 x direction and 513 points in the z direction, with grid spacings of $\Delta x = \Delta z = 0.005 \text{ m}$.
 520 The linearity criteria were satisfied with $R_\eta \cong 4.8 \times 10^{-5}$ and $R_b \cong 3.8 \times 10^{-3}$. In

521 contrast to the counter-rotating convection rolls seen in the first test, the analytical b
522 and w fields shown in Fig. 4 depict narrow updraft/downdraft pairs straddling the
523 buoyancy discontinuities. Between the narrow updrafts is a broad region of relatively
524 weak ascent. The w and b fields above the cold surface are mirror images of the fields
525 above the warm surface. Note the change in the scales of the x and (especially) the z
526 axes between Figs. 4 and 2: the low-level thermal disturbance in the second test is much
527 shallower than the disturbance in the first test (and is suggestive of $a > 1$). In this
528 second test case we find dramatic differences between the inhomogeneous INC-2 and
529 homogeneous HNC-2 cases. Specifically, while the INC-2 and A-2 fields are in excellent
530 agreement, the HNC-2 fields showed no signs of even approaching a steady state. Long
531 after the INC-2 simulation had reached a steady state, the HNC-2 fields continued to
532 amplify and develop asymmetric structures associated with flow nonlinearities. The very
533 close agreement between the A-2 solution and the steady state in the INC-2 simulation
534 is shown for the u field in Fig. 5. The u field in the disastrous HNC-2 simulation, at a
535 time when a steady state had already been attained in the INC-2 simulation, is shown
536 in Fig. 6.

537

538 **4 Summary**

539 The linearized Boussinesq equations for the motion of a viscous stably stratified fluid
540 are solved analytically for a surface buoyancy that varies laterally as a square wave.

541 The solution describes two-dimensional laminar convective structures such as thermal
542 convective rolls and updraft/downdraft pairs. The main applications of the solution may
543 be in code verification and the evaluation of different implementations of the surface
544 pressure condition for the pressure Poisson equation. Tests have been conducted for
545 cases where the aspect ratios of the thermal disturbance have been large and small.
546 With attention restricted to disturbances of sufficiently small amplitude, the linear
547 solution and numerically simulated fields with the inhomogeneous Neumann condition
548 for pressure (which is appropriate in the context of the particular fractional step
549 procedure adopted in our DNS code) have been found to be in excellent agreement for
550 both tests. However, in tests with a mis-specified Neumann condition, an excellent
551 agreement with the analytical solution has been found only for the deep (small aspect
552 ratio) disturbance case; errors in the shallow (large aspect ratio) disturbance case have
553 been catastrophic.

554 **Appendix A: Comment on the pressure condition at a lower solid surface**

555 Consider a **three-dimensional** Boussinesq system with equation of motion,

$$556 \quad \frac{\partial \mathbf{u}}{\partial t} = -\nabla \Pi + \nu \nabla^2 \mathbf{u} + \mathbf{F}. \quad (\text{A1})$$

557 Here **$\mathbf{u} = (u, v, w)$** is the **three-dimensional** velocity vector, Π is a kinematic pressure
 558 perturbation, ν is the kinematic viscosity coefficient, and \mathbf{F} is the sum of nonlinear
 559 acceleration and buoyancy terms. Applying the incompressibility condition,

$$560 \quad \nabla \cdot \mathbf{u} = 0, \quad (\text{A2})$$

561 in the equation that results from taking the divergence of (A1) (e.g., Orszag et al., 1986)
 562 yields the Poisson equation,

$$563 \quad \nabla^2 \Pi = \nabla \cdot \mathbf{F}. \quad (\text{A3a})$$

564 Although (A1) and (A2) imply (A3a), the reverse statement is not generally true.
 565 Indeed, eliminating Π from between (A3a) and the equation arising from taking the
 566 divergence of (A1) yields the diffusion equation $\partial \delta / \partial t = \nu \nabla^2 \delta$ for the velocity
 567 divergence $\delta \equiv \nabla \cdot \mathbf{u}$, whose solution is (A2) only if δ is zero initially and on all
 568 boundaries (Orszag et al., 1986; Gresho and Sani, 1987, **Vreman 2014**).

569 The same steps leading to (A3a) also lead to an alternative Poisson equation,

$$570 \quad \nabla^2 \Pi = \nabla \cdot (\nu \nabla^2 \mathbf{u} + \mathbf{F}). \quad (\text{A3b})$$

571 Although $\nabla \cdot \nu \nabla^2 \mathbf{u}$ was omitted in (A3a) [this term is zero if (A2) is satisfied], **without**
 572 **further constraints on δ** (described above), (A2) may not be satisfied. Gresho and Sani

573 (1987) showed that the retention of $\nabla \cdot \nu \nabla^2 \mathbf{u}$ in (A3b) assures that (A2) is satisfied,
574 and thus leads to the paradox: "If you include it, you don't need it; if you don't include
575 it, you need it." Vreman (2014) revisited this paradox, and showed that for a standard
576 staggered method, the discretized form of (A3b) is equivalent to that of (A3a)
577 supplemented with the constraint that $\nabla \cdot \nabla^2 \mathbf{u} = 0$ ($\nabla^2 \delta = 0$) on points adjacent to the
578 solid boundary [with the same inhomogeneous Neumann boundary condition for Π
579 implied for (A3a) and (A3b)]. When supplemented with this $\nabla^2 \delta = 0$ near-wall
580 condition, the diffusion equation for δ led to $\delta = 0$ for all time. We note that (A3b) is
581 the form adopted in our numerical code.

582 Evaluating the vertical component of (A1) on the surface, where the
583 impermeability condition applies, yields the inhomogeneous Neumann condition,

$$584 \quad \left. \frac{\partial \Pi}{\partial z} \right|_0 = \nu \left. \frac{\partial^2 w}{\partial z^2} \right|_0 + F_z \Big|_0, \quad (\text{A4})$$

585 where $w \equiv \mathbf{k} \cdot \mathbf{u}$, $F_z \equiv \mathbf{k} \cdot \mathbf{F}$, \mathbf{k} is the upward unit vector, and $(\) \Big|_0$ is a surface value. It
586 has been argued that (A4), by itself, is not a proper boundary condition because it does
587 not provide new information (it is not independent of the governing equations) and does
588 not enforce the incompressibility condition (A2) at the boundary (Strikwerda, 1984;
589 Henshaw, 1994; Sani et al., 2006). However, as pointed out by Henshaw (1994), many
590 studies that impose (A4) (or a variant of it) also apply (A2) on the boundary.

591 In our numerical model, (A1) is integrated using a fractional step procedure with

592 explicit treatment of the viscous term. First, a provisional velocity field $\tilde{\mathbf{u}}$ that does not
 593 satisfy (A2) is obtained by integrating a discretized form of (A1) in which the pressure
 594 gradient is omitted. The provisional velocity is equal to the velocity at the end of the
 595 previous time step plus the sum of the forcing terms (nonlinear acceleration, buoyancy,
 596 and viscous stress) multiplied by the time step Δt . With the forcing terms explicitly
 597 evaluated, $\tilde{\mathbf{u}}$ is readily computed throughout the flow domain, including on the surface,
 598 where, in surface-forced flows, the buoyancy will make a substantial contribution. In
 599 terms of $\tilde{\mathbf{u}}$ and its vertical component \tilde{w} , (A3b) and (A4) become,

$$600 \quad \nabla^2 \Pi = \frac{\nabla \cdot \tilde{\mathbf{u}}}{\Delta t}, \quad (\text{A5})$$

$$601 \quad \left. \frac{\partial \Pi}{\partial z} \right|_0 - \frac{1}{\Delta t} \tilde{w} \Big|_0 = 0. \quad (\text{A6})$$

602 In the second step, a velocity field that does satisfy (A2) is obtained by solving (A5) for
 603 Π and then adding the pressure gradient force associated with Π (multiplied by Δt) to
 604 $\tilde{\mathbf{u}}$.

605 In some explicit fractional step procedures (including the DNS code used in our
 606 study), the problem of solving (A5) subject to (A6) with $\tilde{\mathbf{u}}|_0$ evaluated from model data
 607 is replaced by what appears to be an entirely different (but is actually equivalent)
 608 problem: solving (A5) subject to the homogeneous Neumann condition,

$$609 \quad \left. \frac{\partial \Pi}{\partial z} \right|_0 = 0, \quad (\text{A7})$$

610 in concert with $\tilde{\mathbf{u}}|_0$ being set to 0, obviating the need to calculate $\tilde{\mathbf{u}}|_0$ from model data.

611 It can be shown that $\tilde{w}|_0$ and the discretized form of $\partial\Pi/\partial z|_0$ appear in the discretized

612 form of (A5) valid half a grid point above the physical surface as $\partial\Pi/\partial z|_0 - \tilde{w}|_0/\Delta t$, that

613 is, in the same combination as they appear in (A6). Thus, setting $\tilde{w}|_0$ and $\partial\Pi/\partial z|_0$ to 0,

614 is equivalent to implementing (A6) with the model-computed values of $\tilde{w}|_0$: the

615 discretized form of (A5) near the surface is the same in either case. Moreover, on the C

616 grid, setting the tangential components $\tilde{u}|_0$ and $\tilde{v}|_0$ to 0 only affects the values of \tilde{u} and

617 \tilde{v} half a grid point beneath the physical boundary. These values do not appear in the

618 discretized form of (A5) at any z -level, and thus have no bearing on the solution. In

619 essence, the errors associated with the conflation of the two physically unjustifiable

620 specifications (homogeneous Neumann condition for pressure, and $\tilde{\mathbf{u}}|_0 = 0$) cancel out.

621 The homogeneous Neumann condition for pressure can be the source of confusion

622 if the context in which the condition is applied is not made clear: it would be a correct

623 condition if $\tilde{\mathbf{u}}|_0$ is set to zero (per the equivalence described above), but it would be an

624 incorrect condition if the explicit model-computed values of $\tilde{\mathbf{u}}|_0$ are used. In the

625 experiments with the mis-specified condition described in Sect. 3, the homogeneous

626 condition is imposed in the latter context. Unfortunately, in many numerical model

627 descriptions, the nature of the surface pressure condition is left vague, for example, by

628 not indicating whether a Neumann condition is homogeneous or inhomogeneous, or, if a
629 homogeneous Neumann condition is indicated, not mentioning how $\tilde{\mathbf{u}}|_0$ is treated.

630 Finally, we note that in fractional step procedures that treat the viscous term
631 implicitly (e.g., Kim and Moin, 1985; Gresho, 1990; Armfield and Street, 2002;
632 Guermond et al., 2006, and many others), the homogeneous Neumann condition is often
633 applied as a surface condition for a Poisson equation, but it is again different from our
634 implementation described in Sect. 3. In the implicit treatments, the provisional velocity
635 is obtained as the solution of a boundary value problem ($\tilde{\mathbf{u}}|_0$ should be specified; often
636 it is set to 0) in which the relevant Poisson equation resembles (A5) but applies to a
637 scalar function (sometimes called a pseudo-pressure) that is not the real pressure.
638 Temam (1991) refers to this scalar as, "... a technical quantity, a mathematical
639 auxiliary..." and advocates that it should not even be considered as an approximation of
640 the pressure. Interestingly, in the context of implicit treatments, the homogeneous
641 Neumann condition on the pseudo-pressure has sometimes been implicated as corrupting
642 solution accuracy through the development of spurious numerical boundary layers
643 adjacent to solid boundaries (Gresho, 1990; Guermond et al., 2006; Hosseini and Feng,
644 2011).

645

646 **Code availability**

647 The Fortran program used to generate output data files from the analytical solution is

648 available as a supplement to this article. That program (square.f) is configured for test
649 A-1, but can be easily adjusted to run test A-2 or other tests. Running square.f
650 automatically generates an output file for each dependent variable (e.g., u.dat) as well
651 as an output file (square.out) that summarizes the test parameters and gives the
652 computed values of the linearity ratios R_η and R_b defined in (3.1).

653

654 *Acknowledgements.* This research was supported by the National Science Foundation
655 under Grant AGS-1359698. Comments by Chiel van Heerwaarden, Juan Pedro Mellado,
656 Inanc Senocak, and an anonymous reviewer are gratefully acknowledged.

657 **References**

- 658 Armfield, S. and Street, R.: An analysis and comparison of the time accuracy of
659 fractional-step methods for the Navier-Stokes equations on staggered grids. *Int.*
660 *J. Numer. Methods Fluids*, 38, 255–282, 2002.
- 661 Atkinson, B.: *Meso-scale Atmospheric Circulations*. Academic Press. 495 pp., 1981.
- 662 Axelsen, S. L., Shapiro, A., and Fedorovich, E.: Analytical solution for katabatic flow
663 induced by an isolated cold strip. *Environ. Fluid Mech.*, 10, 387–414, 2010.
- 664 Briggs, G. A.: Surface inhomogeneity effects on convective diffusion. *Boundary-Layer*
665 *Meteorol.*, 45, 117–135, 1988.
- 666 Chandrasekhar, S.: *Hydrodynamic and Hydromagnetic Stability*. Oxford University
667 Press. 652 pp., 1961.
- 668 Chorin, A. J.: Numerical solution of the Navier-Stokes equations. *Math. Comput.*, 22,
669 745–762, 1968.
- 670 Egger, J.: On the linear two-dimensional theory of thermally induced slope winds. *Beitr.*
671 *Phys. Atmosph.*, 54, 465–481, 1981.
- 672 Fedorovich, E., Nieuwstadt, F. T. M., and Kaiser, R.: Numerical and laboratory study
673 of a horizontally evolving convective boundary layer. Part I: Transition
674 regimes and development of the mixed layer. *J. Atmos. Sci.*, 58, 70–86, 2001.
- 675 Fedorovich, E. and Shapiro, A.: Structure of numerically simulated katabatic and
676 anabatic flows along steep slopes. *Acta Geophys.*, 57, 981–1010, 2009a.

677 Fedorovich, E. and Shapiro, A.: Turbulent natural convection along a vertical plate
678 immersed in a stably stratified fluid. *J. Fluid Mech.*, 636, 41–57, 2009b.

679 Gresho, P. M. and Sani, R. L.: On pressure boundary conditions for the incompressible
680 Navier-Stokes equations. *Int. J. Numer. Methods Fluids*, 7, 1111–1145, 1987.

681 Gresho, P. M.: On the theory of semi-implicit projection methods for viscous
682 incompressible flow and its implementation via a finite element method that also
683 introduces a nearly consistent mass matrix. Part 1: Theory. *Int. J. Numer.*
684 *Methods Fluids*, 11, 587–620, 1990.

685 Guermond, J. L., Mineev, P., and Shen, J.: An overview of projection methods for
686 incompressible flows. *Comput. Methods Appl. Mech. Engrg.* 195, 6011–6045,
687 2006.

688 Hadfield, M. G., Cotton, W. R., and Pielke, R. A.: Large-eddy simulations of thermally
689 forced circulations in the convective boundary layer. Part I: A small-scale
690 circulation with zero wind. *Boundary-Layer Meteorol.*, 57, 79–114, 1991.

691 Henshaw, W. D: A fourth-order accurate method for the incompressible Navier-Stokes
692 equations on overlapping grids. *J. Comput. Phys.*, 113, 13–25, 1994.

693 Hosseini, S. M. and Feng, J. J.: Pressure boundary conditions for computing
694 incompressible flows with SPH. *J. Comput. Phys.*, 230, 7473–7487, 2011.

695 Kang, S.-L., Lenschow, D., and Sullivan, P.: Effects of mesoscale surface thermal
696 heterogeneity on low-level horizontal wind speeds. *Boundary-Layer Meteorol.*,

697 143, 409–432, 2012.

698 Kim, J. and Moin, P.: Application of a fractional-step method to incompressible
699 Navier-Stokes equations. *J. Comput. Phys.*, 59, 308–323, 1985.

700 Kundu, P. K.: *Fluid Mechanics*. Academic Press. 638 pp., 1990.

701 Mahrt, L., Sun, J., Vickers, D., MacPherson, J. I., Pederson, J. R., and Desjardins, R.
702 L.: Observations of fluxes and inland breezes over a heterogeneous surface. *J.*
703 *Atmos. Sci.*, 51, 2484–2499, 1994.

704 McPherson, R. A.: A review of vegetation-atmosphere interactions and their influences
705 on mesoscale phenomena. *Prog. Phys. Geog.*, 31, 261–285, 2007.

706 Nordström, J., Mattsson, K., and Swanson, C.: Boundary conditions for a divergence
707 free velocity-pressure formulation of the Navier-Stokes equations. *J.*
708 *Comput. Phys.*, 225, 874–890, 2007.

709 Orszag, S. A., Israeli, M., and Deville, M. O.: Boundary conditions for incompressible
710 flows. *J. Sci. Comput.*, 1, 75–111, 1986.

711 Patton, E. G., Sullivan, P. P., and Moeng, C.-H.: The influence of idealized
712 heterogeneity on wet and dry planetary boundary layers coupled to the land
713 surface. *J. Atmos. Sci.*, 62, 2078–2097, 2005.

714 Petersson, N. A.: Stability of pressure boundary conditions for Stokes and Navier-
715 Stokes equations. *J. Comput. Phys.*, 172, 40–70, 2001.

716 Pielke, R. A.: Influence of the spatial distribution of vegetation and soils on the

717 prediction of cumulus convective rainfall. *Rev. Geophys.*, 39, 151–177, 2001.

718 Rempfer, D.: On boundary conditions for incompressible Navier-Stokes problems. *Appl.*
719 *Mech. Rev.*, 59, 107–125, 2006.

720 Segal, M. and Arritt, R. W.: Non-classical mesoscale circulations caused by surface
721 sensible heat-flux gradients. *Bull. Amer. Meteorol. Soc.*, 73, 1593–1604, 1992.

722 Shirokoff, D. and Rosales, R. R.: An efficient method for the incompressible Navier-
723 Stokes equations on irregular domains with no-slip boundary conditions, high
724 order up to the boundary. *J. Comput. Phys.*, 230, 8619–8646, 2011.

725 Shapiro, A. and Fedorovich, E.: Similarity models for unsteady free convection flows
726 along a differentially cooled horizontal surface. *J. Fluid Mech.*, 736, 444–463,
727 2013.

728 Shapiro, A. and Fedorovich, E.: A boundary-layer scaling for turbulent katabatic flow.
729 *Boundary-Layer Meteorol.*, 153, 1–17, 2014.

730 Simpson, J. E.: *Sea Breeze and Local Winds*. Cambridge University Press. 234 pp.,
731 1994.

732 Temam, R.: Remark on the pressure boundary condition for the projection method.
733 *Theoret. Comput. Fluid Dynamics*, 3, 181–184, 1991.

734 Strikwerda, J. C.: Finite difference methods for the Stokes and Navier-Stokes equations.
735 *SIAM J. Sci. Stat. Comput.*, 5, 56–68, 1984.

736 van Heerwaarden, C. C., Mellado, J. P., and de Lozar, A.: Scaling laws for the

- 737 heterogeneously heated free convective boundary layer. *J. Atmos. Sci.*, 71, 3975–
738 4000, 2014.
- 739 Vreman, A. W.: The projection method for the incompressible Navier-Stokes equations:
740 The pressure near a no-slip wall. *J. Comput. Phys.*, 263, 353–374, 2014.

Figure captions

741

742

743 **Figure 1.** Schematic of two-dimensional (x, z) thermal convection induced by a surface
744 buoyancy that varies horizontally (x) as a square wave. Red denotes positive surface
745 buoyancy, blue denotes negative surface buoyancy.

746

747 **Figure 2.** Vertical cross section of the analytical (A-1) buoyancy b and vertical velocity
748 w fields from the first test case. Color bar units are m s^{-2} for b , and m s^{-1} for w .

749

750 **Figure 3.** Vertical cross section of u from the first test case. A-1 is the analytical
751 solution. INC-1 is the numerical simulation with inhomogeneous Neumann condition for
752 pressure. HNC-1 is the numerical simulation with the homogeneous Neumann condition
753 for pressure. Color bar units are m s^{-1} .

754

755 **Figure 4.** Vertical cross section of the analytical (A-2) buoyancy b and vertical velocity
756 w fields from the second test case. Color bar units are m s^{-2} for b , and m s^{-1} for w .

757

758 **Figure 5.** Vertical cross section of u from the second test case. A-2 is the analytical
759 solution. INC-2 is the numerical simulation with inhomogeneous Neumann condition for

760 pressure. Color bar units are m s^{-1} .

761

762 **Figure 6.** Vertical cross section of u from HNC-2, the numerical simulation with
763 homogeneous Neumann condition for pressure in the second test case. Color bar units

764 are m s^{-1} .

765

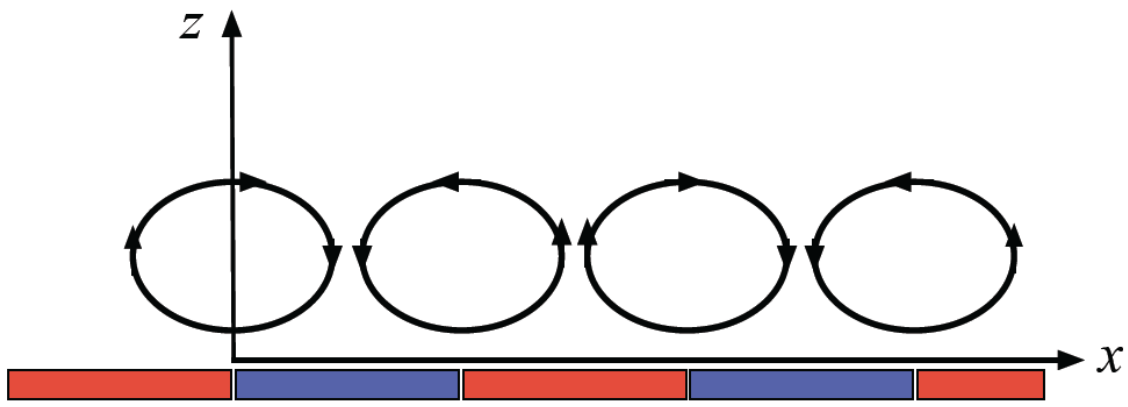
766

767

768

769

770



771

772

773

774

775

776

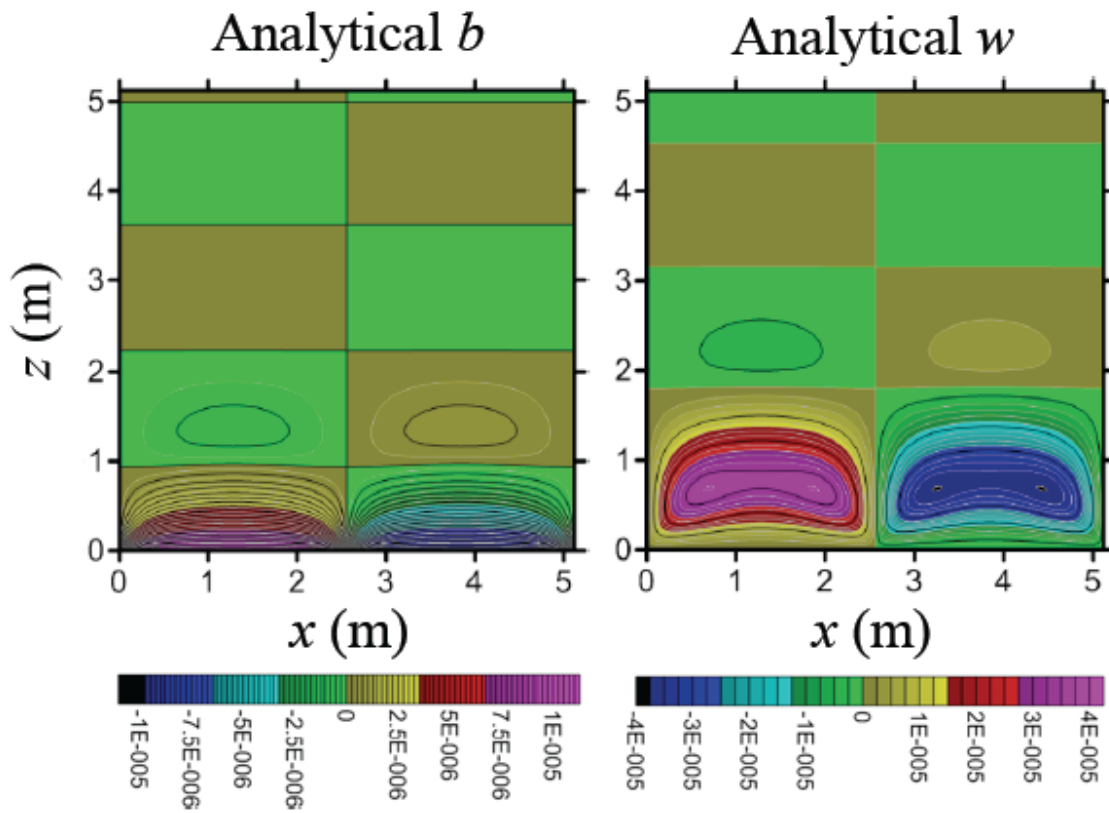
777

778 **Figure 1.** Schematic of two-dimensional (x, z) thermal convection induced by a surface

779 buoyancy that varies horizontally (x) as a square wave. Red denotes positive surface

780 buoyancy, blue denotes negative surface buoyancy.

781



782

783

784

785

786

787 **Figure 2.** Vertical cross section of the analytical (A-1) buoyancy b and vertical velocity

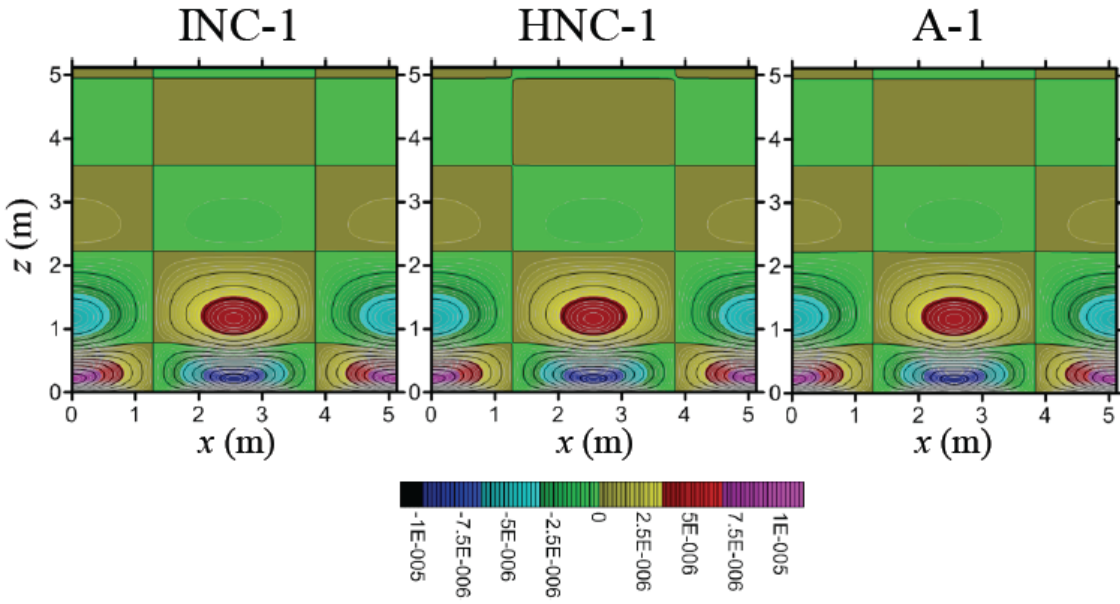
788 w fields from the first test case. Color bar units are m s^{-2} for b , and m s^{-1} for w .

789

790

791

792



793

794

795

796

797

798 **Figure 3.** Vertical cross section of u from the first test case. A-1 is the analytical

799 solution. INC-1 is the numerical simulation with inhomogeneous Neumann condition for

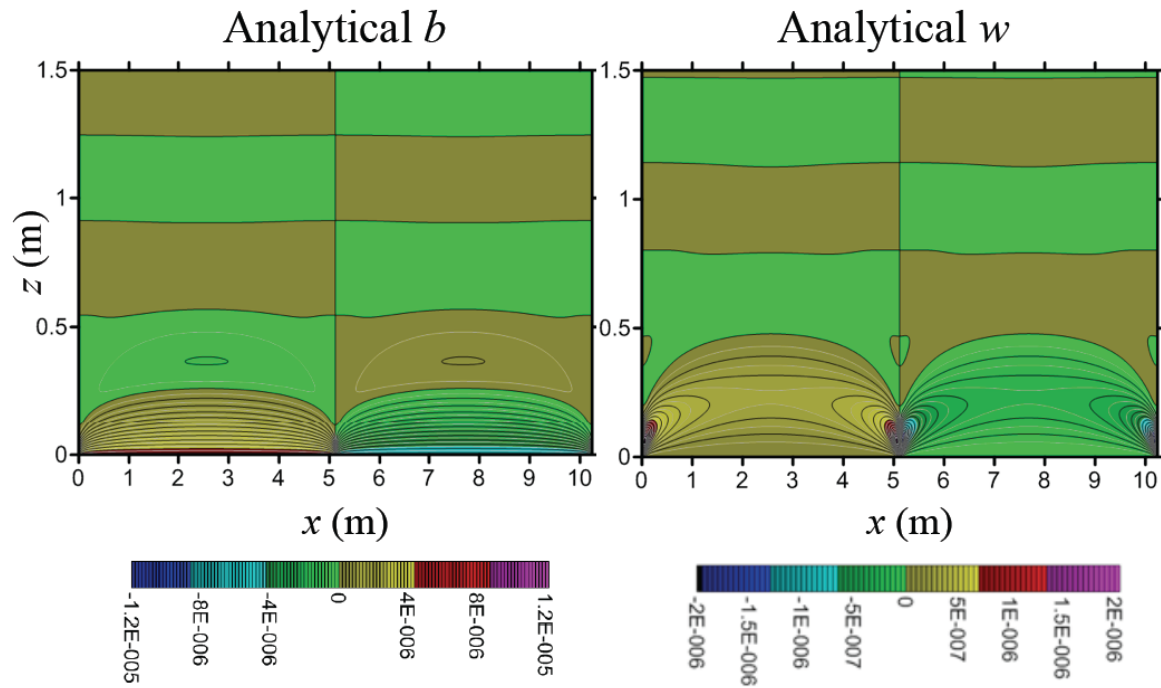
800 pressure. HNC-1 is the numerical simulation with the homogeneous Neumann condition

801 for pressure. Color bar units are m s^{-1} .

802

803

804



805

806

807

808

809 **Figure 4.** Vertical cross section of the analytical (A-2) buoyancy b and vertical velocity

810 w fields from the second test case. Color bar units are m s^{-2} for b , and m s^{-1} for w .

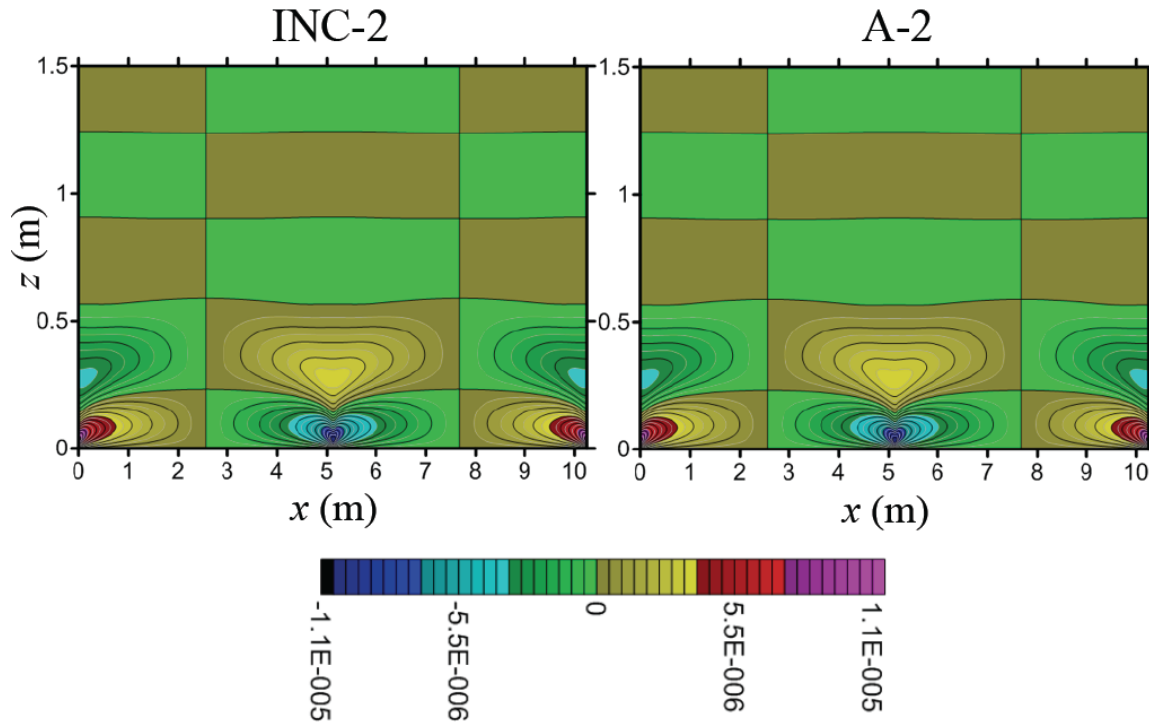
811

812

813

814

815



816

817

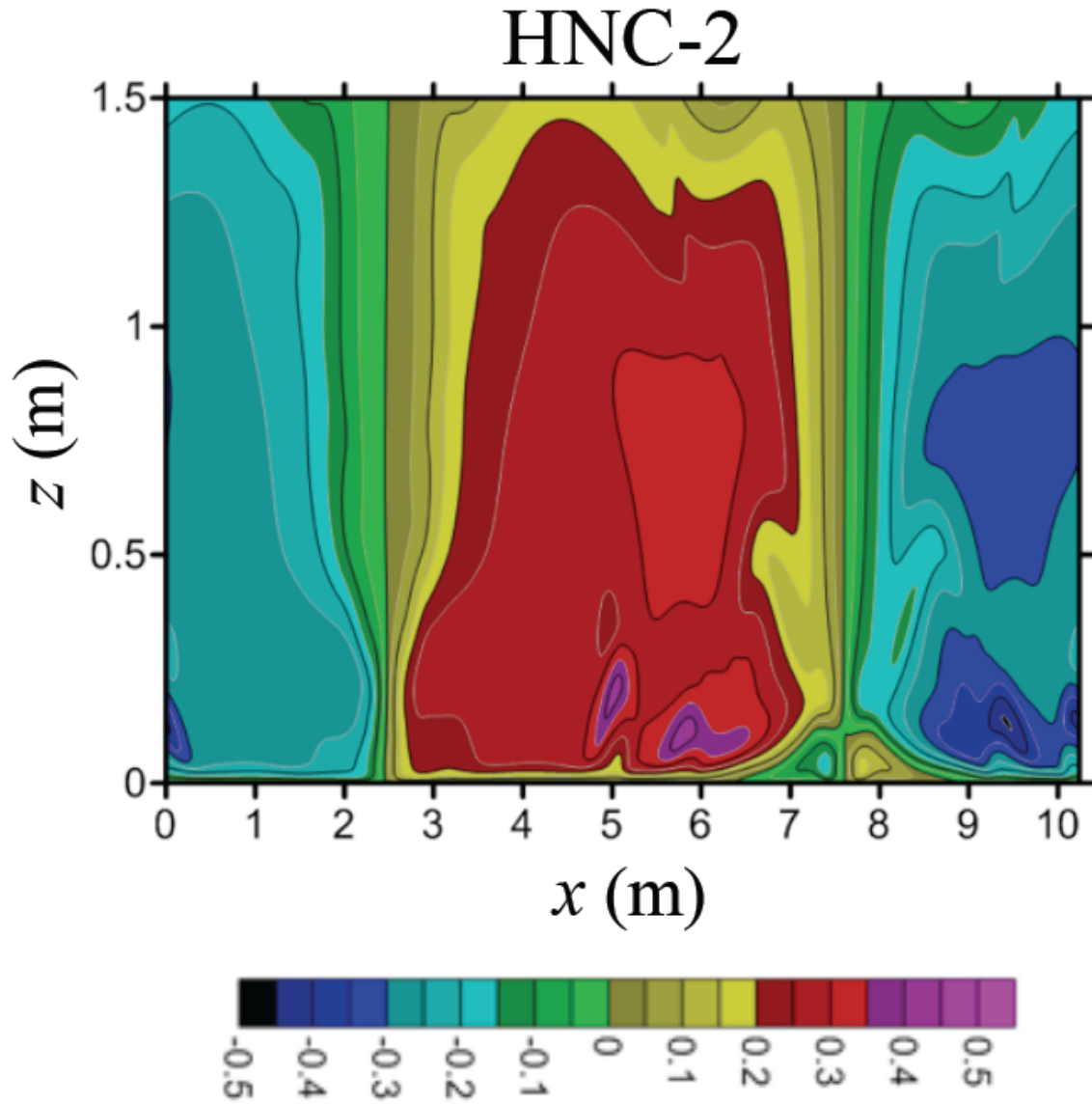
818

819 **Figure 5.** Vertical cross section of u from the second test case. A-2 is the analytical

820 solution. INC-2 is the numerical simulation with inhomogeneous Neumann condition for

821 pressure. Color bar units are m s^{-1} .

822



824

825

826

827 **Figure 6.** Vertical cross section of u from HNC-2, the numerical simulation with

828 homogeneous Neumann condition for pressure in the second test case. Color bar units

829 are m s^{-1} .